micromachines

MDPI

Article

Intensity Switchable and Wide-Angle Mid-Infrared Perfect Absorber with Lithography-Free Phase-Change Film of $Ge_2Sb_2Te_5$

Xiaomin Hua [1] and Gaige Zheng [1,2,*]

[1] Jiangsu Key Laboratory for Optoelectronic Detection of Atmosphere and Ocean, School of Physics and Optoelectronic Engineering, Nanjing University of Information Science & Technology, Nanjing 210044, China; Huahuahuaxiaomin@163.com

[2] Jiangsu Collaborative Innovation Center on Atmospheric Environment and Equipment Technology (CICAEET), Nanjing University of Information Science & Technology, Nanjing 210044, China

* Correspondence: eriot@126.com

Received: 13 May 2019; Accepted: 2 June 2019; Published: 5 June 2019

Abstract: The range of fundamental phenomena and applications achievable by metamaterials (MMs) can be significantly extended by dynamic control over the optical response. A mid-infrared tunable absorber which consists of lithography-free planar multilayered dielectric stacks and germanium antimony tellurium alloy ($Ge_2Sb_2Te_5$, GST) thin film was presented and studied. The absorption spectra under amorphous and crystalline phase conditions was evaluated by the transfer matrix method (TMM). It was shown that significant tuning of absorption can be achieved by switching the phase of thin layer of GST between amorphous and crystalline states. The near unity (>90%) absorption can be significant maintained by incidence angles up to 75 under crystalline state for both transverse electric (TE) and transverse magnetic (TM) polarizations. The proposed method enhances the functionality of MMs-based absorbers and has great potential for application to filters, emitters, and sensors.

Keywords: perfect absorption; phase-change materials; silicon carbide; lithography-free

1. Introduction

The realization of a metamaterials absorber (MMA) has long been a goal in engineering the spectral absorption properties of nanostructures [1–3]. MMAs have demonstrated the achievement of near-unity absorption in nearly any range of the electromagnetic (EM) spectrum and may be added to the list of unique EM responses achievable with MMs [3–6]. It is usually difficult to meet the requirements of various specific absorption frequencies, but MMAs can overcome this problem by choosing appropriate structural parameters and integrating active materials [7]. Active control over MMs response can pave the way towards novel optical components like tunable polarizers, sensors, and switches [8–12]. So far, many studies have demonstrated that hybridizations of active media with metallic resonating components can be implemented for further control over the resonant property. Graphene [13,14], liquid crystals [15], and phase-change materials (PCM) [16–19] have been introduced into MM systems to facilitate a reconfigurable response. The control of graphene permittivity can be achieved with an external gate voltage, thus the integration of graphene into MMs allows for spectrally tunable absorption. Liquid crystals have been used successfully in MMs, as have metasurfaces (MSs) for the tuning of the spectral positions of the resonances using its reorientation by external electric fields. Recently, Tittl et al. used germanium antimony tellurium alloy (GST) to achieve a switchable plasmonic perfect absorber in the mid-infrared ranges (MIR) [20,21].

Spectral controlling and shaping with nanostructures in the MIR region is a hot topic because of the advances in applications such as biochemical sensing, imaging, IR labelling, and so on [22–24]. The fast switching between amorphous and crystalline phases of GST makes it a candidate for active MIR photonic devices. The optical properties of GST, specifically its permittivity, vary considerably between amorphous and crystalline phases. Consequently, GST can readily be harnessed and resonantly enhanced in a nanostructure to realize specific switching characteristics [25–27]. Moreover, MM- and MS-based absorbers often require rather complex, time-consuming nanofabrication steps, and expensive technical equipment, which limit their practical applications.

In this contribution, we adopted phase-change material (PCM) to design a tunable MIR absorber. The key idea was implemented with an overcladding layer of the PCM GST, which provides the great potential not only to overcome the roadblock of a much easier manufacturing process, but also to dynamically adjust the absorption in the MIR. The switchable and wavelength-selective absorption/emissivity can be accomplished by altering the GST phase states as well as the structural parameters of the Ge/ZnS multilayer. The high contrast in the optical properties of GST enabled thermal tuning of the resonant response with modulation depths of >90%.

2. Model and Methods

To approach the construction of an MMA, a numerical investigation into a planar multilayer stack with SiC as the substrate was conducted. As depicted in Figure 1a, PCM GST was deposited on SiC substrate separated by a Ge/ZnS distributed Bragg reflector (DBR). The cross-session view in the x-z plane is displayed in Figure 1b where a, h_1, and h_2 represent the thicknesses of the GST layer, ZnS layer, and Ge layer, respectively. The transverse magnetic (TM) wave is defined as the light source and normally incidents to the stack in this study unless clarified. The GST exhibited two stable structural phases—under the external stimulus, a reversible phase transition between amorphous (aGST) and crystalline (cGST) was experienced. aGST is a lossless dielectric and cGST is a low-lossy dielectric [26]. Within the considered wavelength range (10–12 μm), the refractive index (n) of aGST and cGST was approximately 4.3 and 6.3, respectively. As for the extinction coefficient (k), aGST was near zero and can be regarded as the transparent dielectric, whereas cGST was about 0.6 and had the relatively higher optical loss [28]. The refractive indices of Ge and ZnS are from Palik's optical constants handbook [29] and the literature [30], respectively. In the absence of free charge carriers, the optical properties of SiC is given by the Drude–Lorentz model [31]:

$$\varepsilon_{SiC} = \varepsilon_\infty \frac{\omega^2 - \omega_{LO}^2 + i\gamma\omega}{\omega^2 - \omega_{TO}^2 + i\gamma\omega} \tag{1}$$

where ω_{LO} and ω_{TO} represent the longitudinal and transverse optical phonon frequencies, chosen as 972 cm^{-1} and 796 cm^{-1}, respectively, ε_∞ is set as the high frequency dielectric constant, and γ is defined as the damping rate due to vibrational anharmonicity. In this work, ε_∞ was chosen as 3.75 cm^{-1} and γ was set as 6.5.

The theoretical investigation of this configuration is based on the transfer matrix method (TMM) [32,33]. This method involves two different matrices: One is the transmission matrix and the other is the propagation matrix, which can be described as:

$$\mathrm{TM}_l = \frac{1}{t_l}\begin{bmatrix} 1 & r_l \\ r_l & 1 \end{bmatrix}, \tag{2}$$

$$\mathrm{PM}_l = \begin{bmatrix} \exp(-in_l d_l \omega/c)\ 0 \\ 0\ \exp(in_l d_l \omega/c) \end{bmatrix}. \tag{3}$$

Here, t_l and r_l denote the transmission and reflection coefficients of light transmission from the l-th layer to the (l + 1)-th layer, respectively, which can be derived from the Fresnel equation; d_l is the thickness of the l-th layer. The transmission matrix of this composition can be described as

$$M = \prod_{l} \mathrm{TM}_l \cdot \mathrm{PM}_l. \quad (4)$$

Subsequently, the transmission, reflection, and absorption of this composition can be respectively described as $T = |1/M_{11}|^2$, $R = |M_{21}/M_{11}|^2$, and $A = 1 - T - R$.

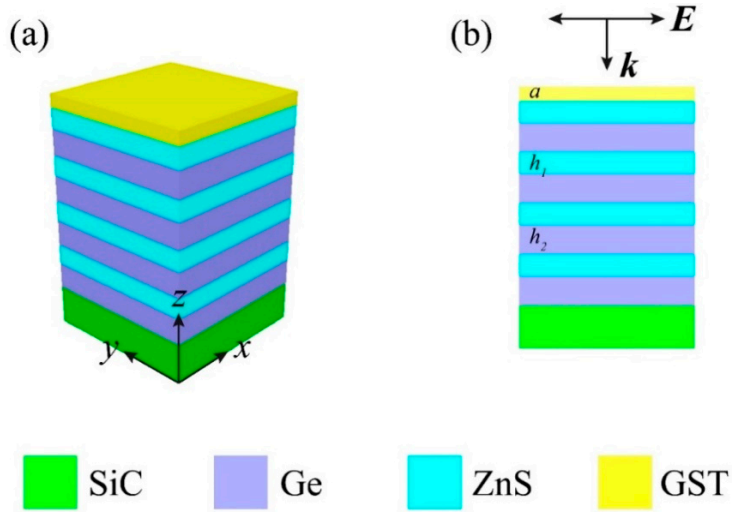

Figure 1. (**a**) Schematic of the initial structure; (**b**) cross-section view of the proposed absorber.

3. Results and Discussions

Phase-change switchable MMs typically comprise of a metallic layer structured with an active PCM layer. Either enhancement or suppressant of resonances in the structured layer can be realized. For the GST, the dielectric constants can change dramatically once the phase transition is initiated by the thermal filed. Figure 2 shows the absorption spectrum of the device for both amorphous (blue curve) and crystalline (red curve) GST. During the structural transition, the absorption underwent an intensity enhancement with a peak at the resonance wavelength of 11.34 μm.

Thus, the absorption can switch between two separate phases of GST. The dynamic absorption control in the presented structure represents a distinct advantage over passive infrared absorbers and emitters [22,34–36].

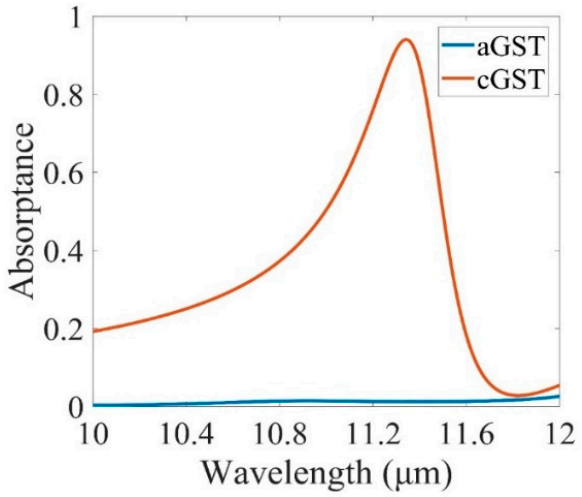

Figure 2. Total absorption at normal incidence for structure with amorphous (aGST) and crystalline (cGST) stable structural phases. The geometrical parameters are originally assumed as a = 0.3 μm, h_1 = 0.53 μm, h_2 = 0.81 μm. Unless otherwise stated, they are used throughout the paper.

The simulated electric field (|E|) distributions on- and off-resonance when the GST is in the amorphous and crystalline phases are shown in Figure 3. It is clear that the strong electric fields were concentrated within a certain region, the field profile of the typical waveguide mode was generated as well. The field enhancement factors at the waveguide-GST interfaces were as high as ~6 under crystalline state (Figure 3b). This increased field intensity led to enhanced absorption at resonant wavelength. Compared with Figure 3a, the low value of the electric field intensity in the Ge/ZnS multilayer with amorphous state resulted in a high reflection.

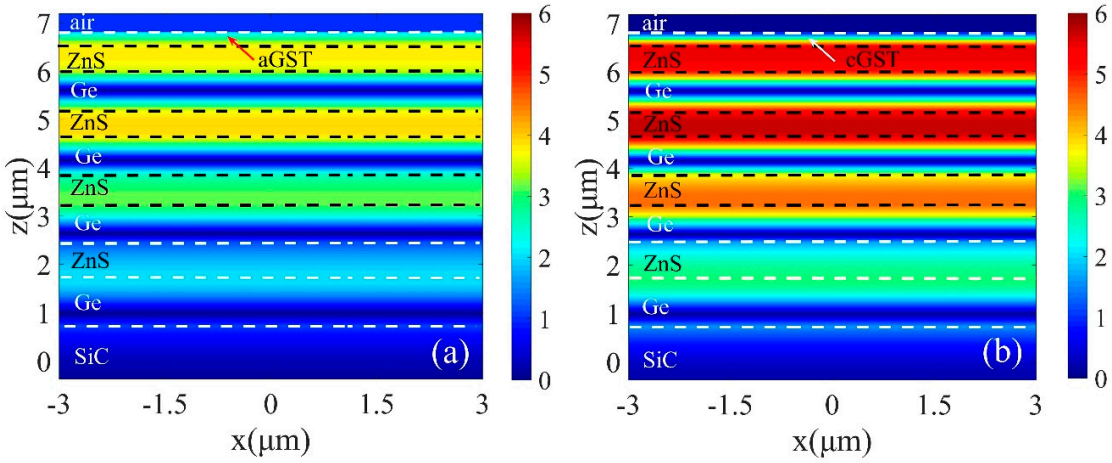

Figure 3. Electric field distribution profiles at the resonance wavelength of 11.34 μm in *x*-*z* plane with (**a**) amorphous (aGST) and (**b**) crystalline (cGST) stable structural phases, respectively.

Absorption spectra of designs with different GST thicknesses (0.15, 0.225, 0.3, 0.375, and 0.45 μm) is shown in Figure 4. The maximum absorption for cGST thickness of 0.15, 0.225, 0.3, 0.375, and 0.45 μm was 0.89, 0.93, 0.94, 0.94, and 0.95, respectively, and the resonance wavelengths were 10.63, 11.09, 11.34, 11.5, and 11.61 μm, respectively. The full width at half-maximum (FWHM) of structures for GST thickness of 0.15, 0.225, 0.3, 0.375, and 0.45 μm were 1.05, 0.76, 0.39, 0.33, and 0.26 μm, respectively, indicating quality factors ($Q = \lambda_0/\Delta\lambda$; λ_0 is the peak wavelength, $\Delta\lambda$ is the FWHM) of 10.12, 14.59, 29.08, 34.85, and 44.65, respectively. The numerical results showed that over 90% peak absorption was maintained when *a* ranged from 0.15 to 0.45 μm at the crystalline phases with other parameters fixed. The resonance wavelength met a red-shift with the increase of *a*, thus the spectral selectivity of the structure was improved.

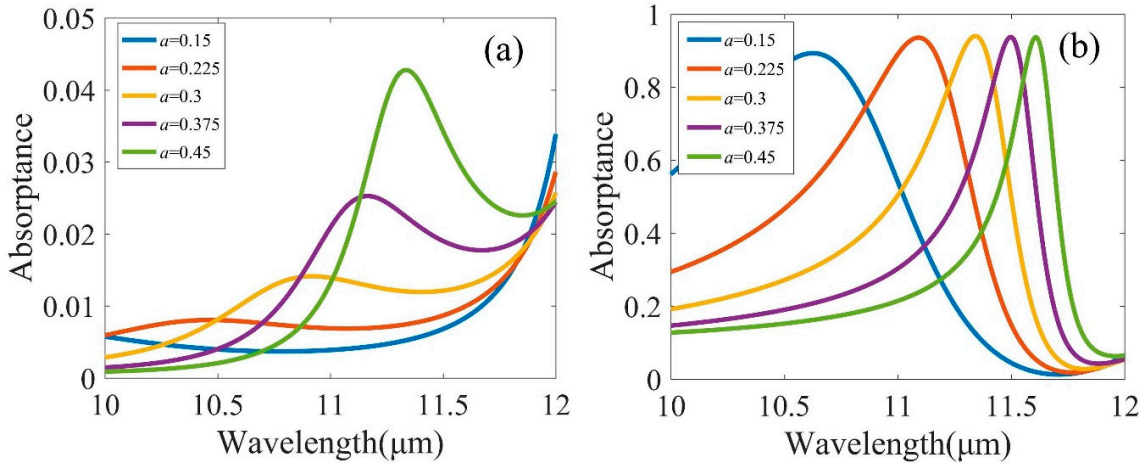

Figure 4. Absorption spectra for various height of (**a**) GST with amorphous (aGST) and (**b**) crystalline (cGST) stable structural phases, respectively. Other geometric parameters were the same as used in Figure 2.

Optical Tamm state (OTS) is a type of surface mode, which can be excited by the normal incidence of light with a zero inplane wavevector component. OTS is observed at the interface between a photonic crystal and a cGST layer (as shown in Figure 3b). We present the numerical calculation of absorption spectra upon normal incidence of light with different h_1 and h_2 in Figure 5. Both structures consisted of four pairs of Ge and ZnS layers. Spectral position of this resonance was highly sensitive to h_1 and h_2. Red-shifting of the absorption peak with increasing h_1 and h_2 was observed. In designing the perfect absorber with this structure, a convenient approach to tune the resonant wavelength is provided. It was also found that total absorption can be maintained over 90%, which provides the opportunity to tune resonance over a wider range of structural parameters. Dependence of the absorption spectrum on N was investigated and shown in Figure 6. The light absorption increased, and then kept the maximal value (~99.6%) when N was larger than 9.

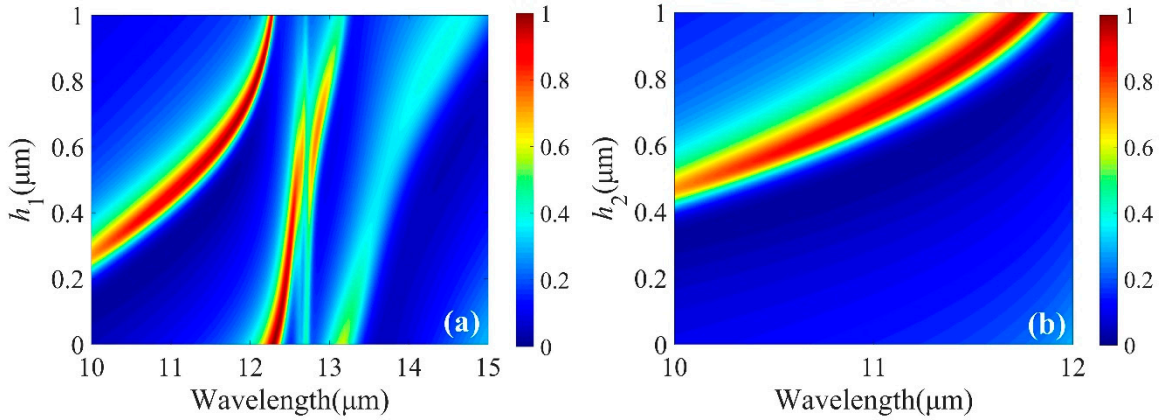

Figure 5. Absorption spectra for various height of ZnS with (**a**) amorphous (aGST) and (**b**) crystalline (cGST) stable structural phases, respectively.

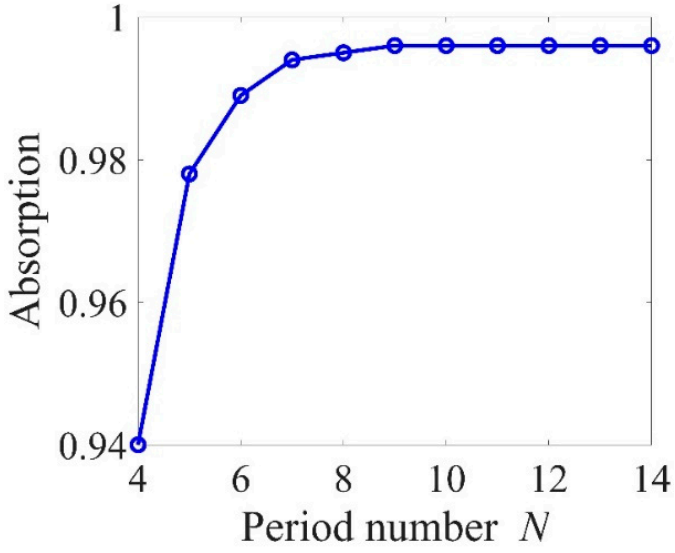

Figure 6. Peak values of light absorption of the structure with period number N when a = 0.3 μm, h_1 = 0.53 μm and h_2 = 0.81 μm.

Figure 7 presents a color-map of absorbance as a function of wavelength and angle of incidence, which is varied from 0° to 90°. Figure 7a,b shows the absorbance in the amorphous phase and crystalline phase for TM polarization while Figure 7c,d gives the absorbance in the amorphous phase and crystalline phase for TE polarization. For both cases, the absorbance was reduced with the increases of incidence angle. The absorbance peak was still larger than 80% at 60°. Moreover, there was a good

spectral overlap between the absorbance for transverse electric (TE) and TM polarizations in each phase state. Therefore, the proposed MMA is polarization independent over a wide range of incident angles.

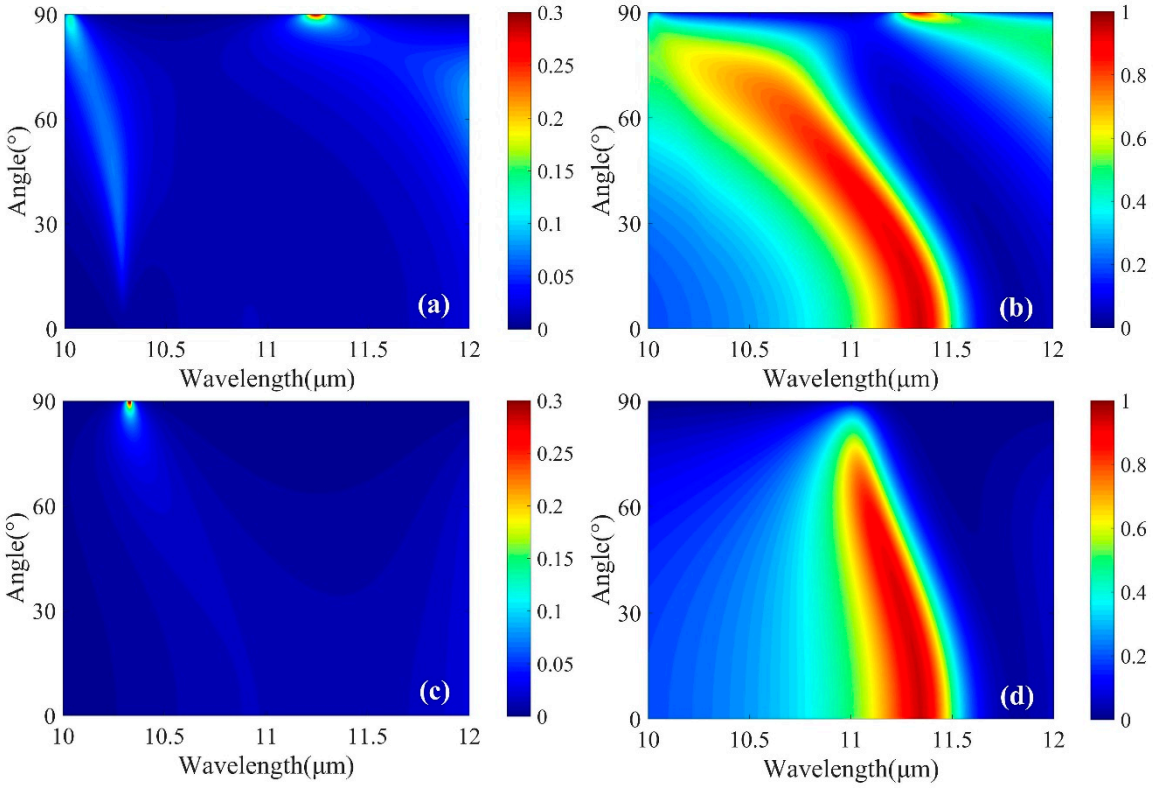

Figure 7. (**a**,**b**) Simulated absorption spectra with different angles of incidence, at the condition of amorphous and crystalline phases for transverse magnetic (TM) polarization, respectively. (**c**,**d**) Simulated absorption spectra with different angles of incidence, at the condition of amorphous and crystalline phases for transverse electric (TE) polarization, respectively. Other geometric parameters are the same as used in Figure 2.

4. Conclusions

In summary, a wavelength-selective polarization independent MMA in the MIR range was proposed using the optical Tamm state surface mode near the GST interface. Compared with previous emphasis on three-dimensional structures, no sophisticated lithography was required, and the resonant absorption bands were tuned by switching the phase of PCM GST between amorphous and crystalline states. This work will find great potential applications in cost-effective active photonic devices.

Author Contributions: Funding acquisition, G.Z.; Investigation, X.H.; Methodology, X.H.; Resources, G.Z.; Software, X.H.; Writing—original draft, X.H.; Writing—review & editing, G.Z.

Funding: This work is partly supported by the National Natural Science Foundation of China (grant number 41675154), Six Major Talent Peak expert of Jiangsu Province (grant number 2015-XXRJ-014, R2016L01) and Jiangsu 333 High-Level Talent Cultivation Program (grant number BRA2016425).

Conflicts of Interest: The authors declare no conflict of interest.

References

1. Cao, L.; White, J.S.; Park, J.S.; Park, J.-S.; Schuller, J.A.; Clemens, B.M.; Brongersma, M.L. Engineering light absorption in semiconductor nanowire devices. *Nat. Mater.* **2009**, *8*, 643–647. [CrossRef]
2. Aydin, K.; Ferry, V.; Briggs, R.M.; Atwater, H.A. Broadband polarization-independent resonant light absorption using ultrathin plasmonic super absorbers. *Nat. Commun.* **2011**, *2*, 517–524. [CrossRef]

3. Liu, X.; Starr, T.; Starr, A.F.; Padilla, W.J. Infrared spatial and frequency selective metamaterial with near-unity absorbance. *Phys. Rev. Lett.* **2010**, *104*, 207403.
4. Tittl, A.; Mai, P.; Taubert, R.; Dregely, D.; Liu, N.; Giessen, H. Palladium-based plasmonic perfect absorber in the visible wavelength range and its application to hydrogen sensing. *Nano Lett.* **2011**, *11*, 4366–4369. [CrossRef]
5. Aslan, E.; Aslan, E.; Turkmen, M.; Saracoglu, O.G. Experimental and numerical characterization of a mid-infrared plasmonic perfect absorber for dual-band enhanced vibrational spectroscopy. *Opt. Mater.* **2017**, *73*, 213–222. [CrossRef]
6. Bang, S.H.; Kim, J.; Yoon, G.; Tanaka, T.; Rho, J. Recent advances in tunable and reconfigurable metamaterials. *Micromachines* **2018**, *9*, 560. [CrossRef]
7. Watts, C.M.; Liu, X.; Padilla, W.J. Metamaterial electromagnetic wave absorbers. *Adv. Mater.* **2012**, *24*, 98–120. [CrossRef]
8. Gu, J.; Singh, R.; Liu, X.; Zhang, X.; Ma, Y.; Zhang, S.; Maier, S.; Tian, Z.; Azad, A.K.; Chen, H.-T.; et al. Active control of electromagnetically induced transparency analogue in terahertz metamaterials. *Nat. Commun.* **2012**, *3*, 1151–1157. [CrossRef]
9. Fan, K.; Padilla, W. Dynamic electromagnetic metamaterials. *Mater. Today* **2015**, *18*, 39–50.
10. Liu, L.; Kang, L.; Mayer, T.S.; Werner, D.H. Hybrid metamaterials for electrically triggered multifunctional control. *Nat. Commun.* **2016**, *7*, 13236.
11. Zhao, X.; Fan, K.; Zhang, J.; Keiser, G.R.; Duang, G.; Averitt, R.D.; Zhang, X. Voltage-tunable dual-layer terahertz metamaterials. *Microsyst. Nanoeng.* **2016**, *2*, 16025–16033.
12. Jung, Y.U.; Bendoym, I.; Crose, D.T. Numerical study of near-, mid-, and long-infrared photon trapping in crystalline and amorphous HgCdTe metamaterials. *Appl. Phys. A* **2016**, *122*, 376–382.
13. Yi, Z.; Chen, J.; Cen, C.; Chen, X.; Zhou, Z.; Tang, Y.; Ye, X.; Xiao, S.; Luo, W.; Wu, P. Tunable graphene-based plasmonic perfect metamaterial absorber in the THz region. *Micromachines* **2019**, *10*, 194–205.
14. Dave, V.; Sorathiya, V.; Guo, T.; Patel, S.K. Graphene based tunable broadband far-infrared absorber. *Superlattices Microst.* **2018**, *124*, 113–120.
15. Yang, L.; Fan, F.; Chen, M.; Zhang, X.; Chang, S.-J. Active terahertz metamaterials based on liquid-crystal induced transparency and absorption. *Opt. Commun.* **2017**, *382*, 42–48.
16. Cao, T.; Wei, C.W.; Simpson, R.E.; Zhang, L.; Cryan, M.J. Broadband polarization-independent perfect absorber using a phase-change metamaterial at visible frequencies. *Sci. Rep.* **2014**, *4*, 3955–3963.
17. Wutting, M.; Bhaskaran, H.; Taubner, T. Phase-change materials for non-volatile photonic applications. *Nat. Photon* **2017**, *11*, 465–476.
18. Torres, D.; Zhang, J.; Dooley, S.; Tan, X.; Sepúlveda, N. Modeling of MEMS mirrors actuated by phase-change mechanism. *Micromachines* **2017**, *8*, 138. [CrossRef]
19. Wang, Q.; Rogers, E.T.F.; Gholipour, B.; Wang, C.-M.; Yuan, G.; Teng, J.; Zheludev, N.I. Optically reconfigurable metasurfaces and photonic devices based on phase change materials. *Nat. Photon.* **2016**, *10*, 60–65.
20. Tittl, A.; Michel, A.-K.U.; Schaferling, M.; Yin, X.; Gholipour, B.; Cui, L.; Wuttig, M.; Taubner, T.; Neubrech, F.; Giessen, H. A switchable mid-infrared plasmonic perfect absorber with multispectral thermal imaging capability. *Adv. Mater.* **2015**, *27*, 4597–4603.
21. Ding, F.; Zhong, S.; Bozhevolnyi, S.I. Vanadium dioxide integrated metasurfaces with switchable functionalities at terahertz frequencies. *Adv. Opt. Mater.* **2018**, *6*, 1701204. [CrossRef]
22. Zhang, Z.; Liang, J.; Zhang, D.; Pang, W.; Zhang, H. A novel bulk acoustic wave resonator for filters and sensors applications. *Micromachines* **2015**, *6*, 1306–1316. [CrossRef]
23. Mohr, D.A.; Yoo, D.; Chen, C.; Li, M.; Oh, S.H. Waveguide-integrated mid-infrared plasmonics with high-efficiency coupling for ultracompact surface-enhanced infrared absorption spectroscopy. *Opt. Express* **2018**, *26*, 23540–23549. [CrossRef]
24. Qu, Y.; Li, Q.; Du, K.; Cai, L.; Lu, J.; Qiu, M. Dynamic thermal emission control based on ultrathin plasmonic metamaterials including phase-changing material GST. *Laser Photonics Rev.* **2017**, *11*, 1700091. [CrossRef]
25. Zhu, N.; Chen, J.; Deng, H.; Di, Y. A graphene-coated mo tip array for highly-efficient nanostructured electron field emitters. *Micromachines* **2018**, *9*, 12. [CrossRef]
26. Zhu, Z.; Evans, P.G.; Haglund, R.F.; Valentine, J.G. Dynamically reconfigurable metadevice employing nanostructured phase-change materials. *Nano Lett.* **2017**, *17*, 4881–4885. [CrossRef]

27. Guo, Z.; Yang, X.; Shen, F.; Zhou, Q.; Gao, J.; Guo, K. Active-tuning and polarization-independent absorber and sensor in the infrared region based on the phase change material of $Ge_2Sb_2Te_5$ (GST). *Sci. Rep.* **2018**, *8*, 12433–12441. [CrossRef]
28. Cai, L.; Du, K.; Qu, Y.; Luo, H.; Pan, M.; Qiu, M.; Li, Q. Nonvolatile tunable silicon-carbide-based midinfrared thermal emitter enabled by phase-changing materials. *Opt. Lett.* **2018**, *43*, 1295–1298. [CrossRef]
29. Palik, E. (Ed.) *Handbook of Optical Constants of Solids*; Academic Press: Waltham, MA, USA, 1998.
30. Bhargava, R.N.; Gallagher, D.; Hong, X.; Nurmikko, A. Optical properties of manganese-doped nanocrystals of ZnS. *Phys. Rev. Lett.* **1994**, *72*, 416–419. [CrossRef]
31. Neuner, B.; Korobkin, D.; Fietz, C.; Carole, D.; Ferro, G.; Shvets, G. Critically coupled surface phonon-polarition excitation in silicon carbide. *Opt. Lett.* **2009**, *34*, 2667–2669. [CrossRef]
32. Kim, T.Y.; Badsha, M.A.; Yoon, J.; Lee, S.Y.; Jun, Y.C.; Hwangbo, C.K. General strategy for broadband coherent perfect absorption and multi-wavelength all-optical switching based on epsilon-near-zero multilayer films. *Sci. Rep.* **2016**, *6*, 22941–22952. [CrossRef]
33. Bhattarai, K.; Ku, Z.; Silva, S.; Jeon, J.; Kim, J.O.; Lee, S.J. A large-area mushroom-capped plasmonic perfect absorber: Refractive index sensing and Fabry-Perot cavity mechanism. *Adv. Opt. Mater.* **2015**, *3*, 1179–1786. [CrossRef]
34. Rude, M.; Simpson, R.; Quidant, R.; Pruneri, V.; Renger, J. Active control of surface plasmon waveguides with a phase change material. *ACS Photon.* **2015**, *2*, 669–674. [CrossRef]
35. Tian, X.; Li, Z. Visible-near infrared ultra-broadband polarization-independent metamaterial perfect absorber involving phase-change materials. *Photo Res.* **2016**, *4*, 146–152. [CrossRef]
36. Ding, F.; Yang, Y.; Bozhevolnyi, S.I. Dynamic metasurfaces using phase-change chalcogenides. *Adv. Opt. Mater.* **2019**. [CrossRef]